Magnetic excitations in the square-lattice iridate Ba_2IrO_4

J. P. Clancy,[1,2] H. Gretarsson,[1] A. Lupascu,[1] J. A. Sears,[1] Z. Nie,[1] M. H. Upton,[3] Jungho Kim,[3] Z. Islam,[3] M. Uchida,[4,*] D. G. Schlom,[5,6] K. M. Shen,[4,6] and Young-June Kim[1]

[1]*Department of Physics, University of Toronto, Toronto, Ontario M5S 1A7, Canada*
[2]*Department of Physics and Astronomy, McMaster University, Hamilton, Ontario L8S 4L8, Canada*
[3]*Advanced Photon Source, Argonne National Laboratory, Argonne, Illinois 60439, USA*
[4]*Laboratory of Atomic and Solid State Physics, Department of Physics, Cornell University, Ithaca, New York 14853, USA*
[5]*Department of Materials Science and Engineering, Cornell University, Ithaca, New York 14853, USA*
[6]*Kavli Institute at Cornell for Nanoscale Science, Ithaca, New York 14853, USA*

(Received 25 March 2022; revised 19 January 2023; accepted 3 February 2023; published 21 February 2023)

We report a resonant inelastic x-ray scattering investigation of ultrathin epitaxial films of Ba_2IrO_4, and compare their low-energy magnetic and spin-orbit excitations to those of their sister compound Sr_2IrO_4. Due to the 180° Ir-O-Ir bond, the bandwidth of the magnon and spin orbiton is significantly larger in Ba_2IrO_4, making it difficult to describe these two types of excitations as separate well-defined quasiparticles. Both types of excitations are found to be quite sensitive to the effect of epitaxial strain. In addition, we find that the d-level inversion observed in Sr_2IrO_4 is absent in Ba_2IrO_4, as predicted in recent theoretical studies. Our results illustrate that the magnetic properties of Ba_2IrO_4 are substantially different from those of Sr_2IrO_4, suggesting that these materials need to be examined more carefully with electron itinerancy taken into account.

DOI: 10.1103/PhysRevB.107.054423

I. INTRODUCTION

Iridium-based transition metal oxides have emerged as a rich source for novel phenomena driven by strong spin-orbit coupling (SOC) effects [1–5]. In particular, the layered perovskite iridate Sr_2IrO_4 is considered as the prototypical $j_{\text{eff}} = \frac{1}{2}$ spin-orbit Mott insulator, whose ground state arises due to a complex interplay between crystal electric field, SOC, and electronic correlation [1]. In addition, the strong parallels between Sr_2IrO_4 and La_2CuO_4, the parent compound of the high T_c cuprates, have led to natural associations with superconductivity [6–9] and have inspired extensive research into the properties of doped Sr_2IrO_4. However, in spite of several theoretical predictions, the experimental realization of iridate superconductivity through chemical substitution has proven elusive [6,7,9]. Physical properties and key issues of Sr_2IrO_4 have been discussed in recent review articles [4,5].

Despite great interest in Sr_2IrO_4, its sister compound Ba_2IrO_4 has received comparatively little experimental attention, largely due to the difficulty of sample synthesis. Since Ba_2IrO_4 is metastable under ambient conditions, high-pressure ($P > 6$ GPa) synthesis is required to obtain bulk Ba_2IrO_4 samples [10]. A quick glance at the existing data seems to suggest that these two compounds are magnetically similar. Ba_2IrO_4 and Sr_2IrO_4 display identical magnetic transition temperatures ($T_N = 240$ K) and very similar magnetically ordered structures [11]. Angle-resolved photoemission (ARPES) and x-ray absorption spectroscopy studies report that the electronic structures of these two compounds are also quite similar [12–14]. This is somewhat surprising given that there exists an important structural difference between the two materials. The IrO_6 octahedra are rigidly aligned in Ba_2IrO_4, just as the CuO_6 octahedra in cuprates, while these octahedra are rotated by ∼11° about the c axis in Sr_2IrO_4. This gives rise to key structural differences in terms of Ir-O-Ir bond angles (180° vs 158°) and local distortions of the IrO_6 octahedra (7% vs 4.5% axial elongation). The straight bond is expected to increase hybridization and make Ba_2IrO_4 more itinerant, which puts into question the applicability of the $j_{\text{eff}} = \frac{1}{2}$ pseudospin model for this material. Indeed, recent theoretical studies have pointed out the shortcomings of the pseudospin model [15] and significant mixing of the t_{2g}, e_g, and oxygen p states [16]. Increased hybridization also suggests a stronger superexchange interaction between the pseudospins in Ba_2IrO_4, which seems to be supported by theoretical calculations [15,17]. A recent two-magnon Raman scattering study also seems to indicate the superexchange in Ba_2IrO_4 is about 20%–30% larger than that in Sr_2IrO_4 [18].

The subtlety of the magnetic anisotropy due to the local distortion was discussed in the theoretical study by Bogdanov and co-workers [19]. On a local level, competition between octahedral distortions and longer-range ligand-field effects from the highly charged Ir^{4+} ions is believed to reverse the order of the low-lying d levels in Sr_2IrO_4, but not in Ba_2IrO_4. The net result is to suppress the effect of the tetragonal distortion in Ba_2IrO_4 [19]. However, the weak Ising exchange anisotropy could not explain the basal plane ordering direction observed experimentally [11], and various additional interactions such as the interlayer exchange interaction [20], single-ion anisotropy, and pseudoquadrupolar interaction [21] have been suggested to explain the magnetic structure. In addition, Solovyev *et al.* suggested that the pseudospin model

[*]Present address: Department of Physics, Tokyo Institute of Technology, Tokyo 152-8551, Japan.

is inadequate for Ba_2IrO_4 due to the increased hybridization, and higher-order terms arising from itinerancy of the system should be considered [15]. Unfortunately, there have been only limited experimental studies on Ba_2IrO_4 to test these theories, mainly due to the difficulty with growing single crystal samples.

In this paper, we examine the magnetic Hamiltonian of Ba_2IrO_4 by studying thin film samples. In the absence of high-quality single crystal samples, thin films provide an important avenue for studying the underlying physics of this material. Epitaxial film growth [14,22,23] offers an elegant alternative to the high-pressure synthesis techniques required for Ba_2IrO_4 [10], providing a method for both stabilizing the crystal structure and exerting a high level of control over key structural parameters. To probe characteristic excitations of such thin film samples, we use resonant inelastic x-ray scattering (RIXS) to map out the dispersion of magnetic and orbital excitations. RIXS is a momentum-resolved and element-specific probe of elementary excitations such as magnons or orbitons [8,24,25]. We compare the RIXS spectra of Ba_2IrO_4 thin film samples with those obtained for Sr_2IrO_4, and found that despite the overall similarity of the magnetic excitation spectra, the magnetic energy scales in Ba_2IrO_4 differ significantly from those in Sr_2IrO_4. The magnon and spin-orbital excitations are no longer well separated in Ba_2IrO_4, making it difficult to justify the use of the pseudospin model to describe magnetic properties. In addition, we confirm that the magnetic anisotropy is reversed in Ba_2IrO_4 as predicted in Ref. [19]. Our results show that the structural differences between square-lattice iridates make the magnetic properties of Ba_2IrO_4 distinct from those of Sr_2IrO_4.

II. EXPERIMENTAL DETAILS

Measurements were performed on two ultrathin Ba_2IrO_4 samples prepared by molecular beam epitaxy: one 20-nm ($\sim$15 unit cells) film grown on a $PrScO_3$ (PSO) substrate, and one 13-nm ($\sim$10 unit cells) film grown on $GdScO_3$ (GSO). A more detailed description of the synthesis procedure can be found in Ref. [14]. Reflection high-energy electron diffraction (RHEED) was used to monitor the films throughout the growth process, and to verify that there was no evidence of lattice relaxation. After synthesis, a combination of low-energy electron diffraction (LEED) and x-ray diffraction was used to confirm the phase purity, crystallinity, and lattice constants of the films. In addition, the ARPES data [14] provide confirmation that the electronic structures of thin film samples are comparable to bulk crystals. The degree of lattice mismatch in these two samples is somewhat different, with the PSO sample approaching unstrained bulk material ($\Delta a/a = -0.2\%$) and the GSO sample exhibiting a sizable compressive strain ($\Delta a/a = -1.4\%$). The effect of epitaxial strain on the crystal structure of Ba_2IrO_4 is illustrated in Fig. 1(a). Bulk single crystals of Sr_2IrO_4 were synthesized using the self-flux technique, as described in Ref. [26]. Throughout this paper, we will compare the RIXS spectra for Ba_2IrO_4 thin film samples with those for Sr_2IrO_4 single crystals. This is justified for the following two reasons. First, the magnetic structure of the thin film samples remains unchanged from that of single crystal samples [27]. Second, we note that Lupascu *et al.* reported that

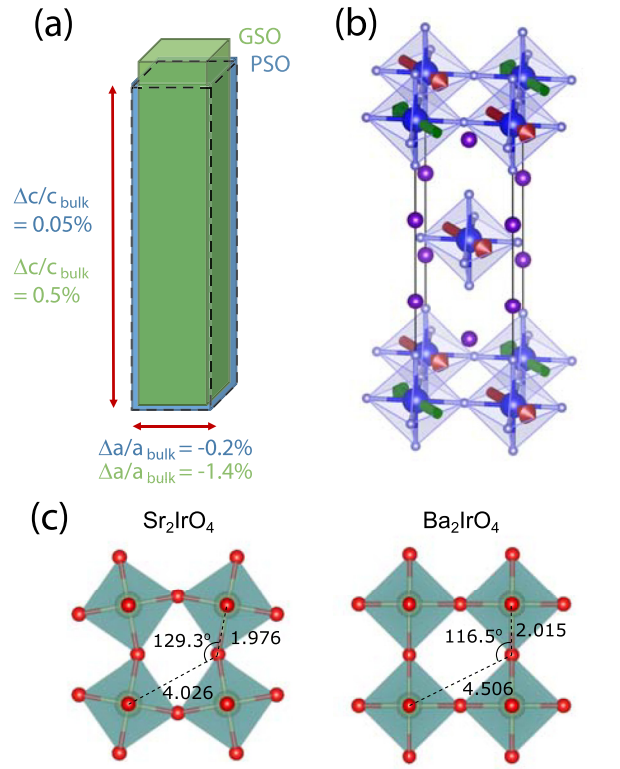

FIG. 1. (a) Effect of epitaxial strain on the crystal structure of Ba_2IrO_4. The unit cell of bulk Ba_2IrO_4 is illustrated by the dashed black lines. Epitaxial strains generated by $PrScO_3$ (PSO, blue) and $GdScO_3$ (GSO, green) substrates have been magnified by a factor of 10. (b) The collinear antiferromagnetic ground state of Ba_2IrO_4. (c) A comparison of Ir-O-Ir bond geometry in Sr_2IrO_4 and Ba_2IrO_4.

RIXS data for thin film Sr_2IrO_4 are quite similar to those for bulk single crystal Sr_2IrO_4 [28]. The zone-boundary magnon energy shifts slightly due to epitaxial strain, but the spin-orbit exciton energy is the same in both thin film and single crystal samples.

Ir L_3-edge RIXS measurements were performed using the MERIX spectrometer on Beamline 30-ID-B at the Advanced Photon Source. A channel-cut Si-(8,4,4) secondary monochromator, and a spherical (2 m radius) diced Si-(8,4,4) analyzer crystal were used to obtain an overall energy resolution of 45 meV [full width at half maximum (FWHM)]. To reduce the strong elastic scattering contribution from the sample and substrate, measurements were carried out in horizontal scattering geometry, with a scattering angle close to $2\theta = 90^\circ$ and at $T = 10$ K. To maximize the inelastic scattering from the films, measurements were performed near grazing incidence, with an angle of incidence $\alpha < 1^\circ$. In this grazing-incidence geometry, the photon polarization is roughly along the crystallographic c direction.

III. EXPERIMENTAL RESULTS

Results from the RIXS measurements on the essentially unstrained film, Ba_2IrO_4 on PSO, are presented in Fig. 2. Figure 2(a) shows representative energy scans collected at

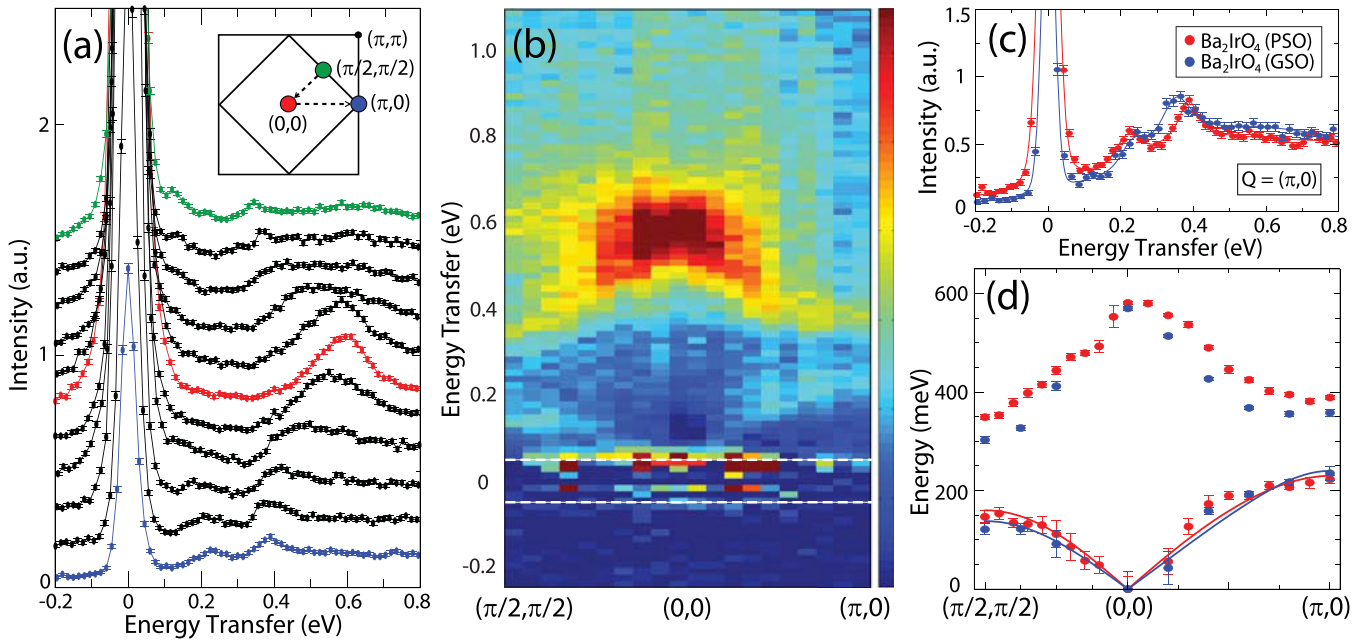

FIG. 2. (a) Representative energy scans performed on 20-nm thin film Ba_2IrO_4 grown on a PSO substrate. Colored spectra were obtained at the high-symmetry points of the magnetic Brillouin zone shown in the inset. The top 5 spectra correspond to the scans obtained along the $(0,0)$-$(\pi/2,\pi/2)$ momentum transfer direction, while the bottom 5 were obtained for $(0,0)$-$(\pi,0)$. Spectra have been offset vertically for illustrative purposes. Inset: The magnetic Brillouin zone for Ba_2IrO_4. (b) Color contour map showing the dispersion of the low-energy magnon (∼0–250 meV) and spin-orbit exciton (∼350–650 meV) modes in Ba_2IrO_4. The elastic scattering contribution has been subtracted from this panel in order to highlight the inelastic features. The position of the elastic line is denoted by dashed white lines. (c) Strain dependence of magnetic and orbital excitations in Ba_2IrO_4 grown on PSO (−0.2% strain, red) and GSO (−1.4% strain, blue) substrates. (d) Dispersion of magnon and spin-orbit exciton modes in thin film Ba_2IrO_4. The magnetic dispersion can be fit to a Heisenberg J-J'-J'' model (solid red and blue lines).

high-symmetry points throughout the magnetic Brillouin zone. Here, the scattering intensity is plotted as a function of energy transfer ΔE. The distinguishing features of these spectra are (1) a strong, resolution-limited elastic line ($\Delta E = 0$), (2) a dispersive magnetic excitation, or magnon, at low energy ($\Delta E < 250$ meV), and (3) a dispersive orbital excitation, or spin-orbit exciton, at higher energy ($350 < \Delta E < 650$ meV). Figure 2(b) shows a color intensity map constructed out of energy scans similar to those of Fig. 2(a). In order to emphasize the inelastic features, the elastic scattering contribution has been subtracted from the data sets.

A direct comparison of Ba_2IrO_4 and Sr_2IrO_4 spectra, obtained under equivalent experimental conditions, is provided in Fig. 3(a). The energy of the magnon mode at $\mathbf{Q} = (\pi, 0)$, which provides a measure of the full magnetic bandwidth, is significantly larger in Ba_2IrO_4 (223 ± 4 meV) than Sr_2IrO_4 (178 ± 4 meV). This difference in bandwidth (∼25%) is qualitatively consistent with predictions based on quantum chemistry calculations by Katukuri *et al.* [17]. One important consequence of the larger bandwidth in Ba_2IrO_4 is the proximity of the magnon mode and the spin-orbiton mode. These two modes are well separated in Sr_2IrO_4, but the larger bandwidth in Ba_2IrO_4 pushes the magnon mode up and the spin-orbiton mode down as shown in Fig. 3(a). This is also clearly shown in the dispersion plot of Fig. 2(d), in which these two modes seem to come close to each other in energy as they approach the $(\pi, 0)$ point. In many other iridates described by the $j_{\text{eff}} = \frac{1}{2}$ picture, the $j_{\text{eff}} = \frac{1}{2}$ and $j_{\text{eff}} = \frac{3}{2}$ states are well separated, meaning that the magnon and spin orbiton can be treated as separate quasiparticles. In Ba_2IrO_4, however, the lack of such a clear separation between the $j_{\text{eff}} = \frac{1}{2}$ and $j_{\text{eff}} = \frac{3}{2}$ states indicates that a full understanding of these collective excitations will require consideration of all six bands in t_{2g} manifolds.

To examine the effect of epitaxial strain on the RIXS spectra, representative energy scans performed on two Ba_2IrO_4 films are plotted in Fig. 2(c). These scans have been collected at the $(\pi, 0)$ zone-boundary position, where the energy of the magnon mode is at its maximum. Note that epitaxial strain does shift the peak positions but the difference is much smaller than that between Ba_2IrO_4 and Sr_2IrO_4 shown in Fig. 3(a). As the magnitude of the compressive strain grows larger, the energy of the magnon mode is enhanced, while that of the spin-orbit exciton mode is reduced. Similar strain-induced tuning of the zone-boundary magnon energy has also been observed in thin film Sr_2IrO_4 [28], where the magnetic bandwidth can be lowered (raised) by the application of a moderate tensile (compressive) strain. However, by measuring the full dispersion of the magnetic excitations, as shown in Fig. 2(d), a more detailed picture of the strain dependence emerges. Each scan at a given momentum was fit using a fit function consisting of elastic-line (resolution-limited pseudo-Voight), magnon (Gaussian), spin-orbit exciton (Lorentzian, Gaussian), and electron-hole continuum/background (broad Gaussian). Only magnon and spin-orbit exciton positions are plotted in Fig. 2(d).

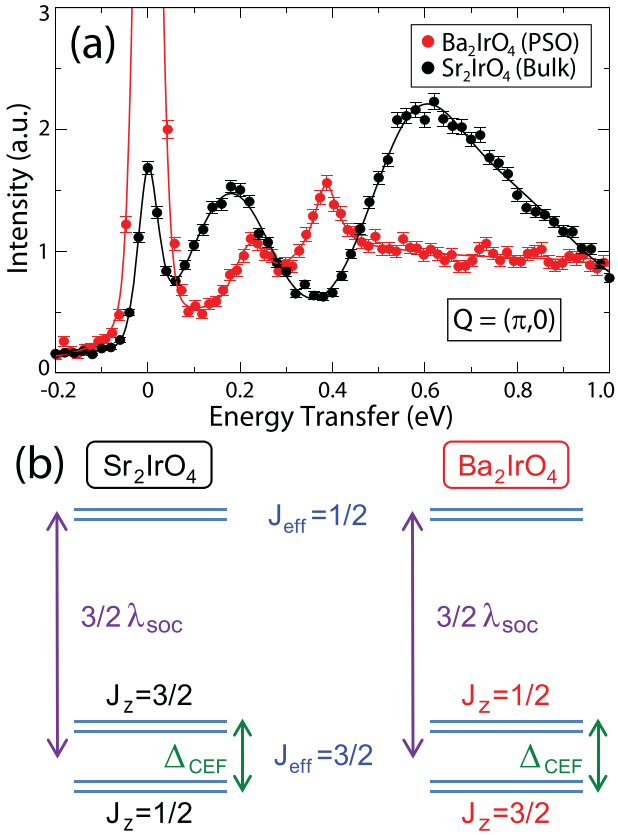

FIG. 3. (a) Representative excitation spectra measured at the $(\pi, 0)$ zone-boundary position for thin film Ba_2IrO_4 (20 nm, PSO substrate) and bulk single crystal Sr_2IrO_4. Both spectra were obtained using grazing incidence geometry. (b) The orbital energy level schemes implied by the spectra in (a). Note that the sign of the noncubic crystal field splitting must be opposite in Ba_2IrO_4 ($\Delta_{CEF} > 0$) and Sr_2IrO_4 ($\Delta_{CEF} < 0$).

IV. DISCUSSION

A. Magnon dispersion relation

To analyze the magnetic dispersion relation, we employ a J-J'-J'' pseudospin model. This is the same phenomenological model which has previously been used to describe magnon dispersion in Sr_2IrO_4 [8] ($J = 60$, $J' = -20$, $J'' = 15$ meV). Substantial ferromagnetic next-nearest coupling was introduced to account for the observed large zone-boundary dispersion. Similarly sizable zone-boundary dispersion is also observed for Ba_2IrO_4, and the dispersion relation is reasonably well described with $J \approx 85$, $J' \approx -15$, $J'' \approx 10$ meV for the PSO film. Similar parameters are also obtained from fitting the GSO film data ($J \approx 82$, $J' \approx -19$, $J'' \approx 16$ meV). The much larger value of J in Ba_2IrO_4 can be understood from the 180° Ir-O-Ir bond angle according to the Goodenough-Kanamori rule. However, the further neighbor interactions in Ba_2IrO_4 are almost as large as the values in Sr_2IrO_4. This is difficult to understand in the superexchange picture, since the next-nearest-neighbor hopping paths in Ba_2IrO_4 are very different from those in Sr_2IrO_4 due to the absence of IrO_6 octahedral rotations [see Fig. 1(c)]. It is possible that superexchange involving $j_{\text{eff}} = \frac{3}{2}$ might account for this, although no such calculation has been reported. However, we would like to point out that the large zone-boundary dispersion could be explained using the so-called ring exchange as discussed in the context of La_2CuO_4 [29], which could indicate considerable electron itinerancy (breakdown of the assumption of large Hubbard U). It should be noted that recent *ab initio* calculations have demonstrated that interplane and symmetric anisotropic interactions are required in order to reproduce the observed magnetic structure of Ba_2IrO_4 [20]. However, the small size of these terms (estimated to be ∼0.5–3.5 meV) means that their contribution to the dispersion is overshadowed by the much stronger in-plane isotropic exchange interactions.

Next, we turn to the effect of epitaxial strain. Although the J-J'-J'' model may not be applicable for Ba_2IrO_4, it is still interesting to compare the obtained exchange interaction parameters. Although compressive strain does serve to increase the overall bandwidth, it actually does so by reducing the nearest-neighbor exchange interaction, while enhancing the second and third neighbor interactions. It is important to remember the structural difference between Ba_2IrO_4 and Sr_2IrO_4 and its effect on the magnetic exchange interactions. This was illustrated in the two-magnon Raman scattering studies of Sr_2IrO_4 thin films by Seo and co-workers [30]. They have reported that the enhanced magnon energy with compressive strain is the result of increased hopping amplitude due to the complexity of the multiorbital nature of the pseudospin. It is interesting to note that a similar suppression of the bandwidth is not observed in the case of Ba_2IrO_4 reported here. A direct comparison of the zone-boundary energy also does not show a difference [Fig. 3(d)]. Perhaps this observation points to the important role of the octahedral rotation in Sr_2IrO_4. However, future two-magnon Raman measurements on Ba_2IrO_4 films could be useful in making a quantitative comparison.

B. Spin-orbital excitations

There are also notable differences in the orbital excitations of these two materials. The spin-orbit exciton mode, originally observed by Kim *et al.* [8], corresponds to excitations between the $j_{\text{eff}} = \frac{3}{2}$ and $j_{\text{eff}} = \frac{1}{2}$ states, which acquire dispersion as they propagate against an antiferromagnetically ordered background. Recent RIXS measurements on Sr_2IrO_4 have demonstrated that this mode exhibits a strong dependence on the photon polarization [31]. When the sample is rotated with respect to the incoming photon polarization, the RIXS matrix elements will change as follows: Scattering from wave functions with a larger in-plane orbital component is enhanced (suppressed) in grazing (normal) incidence, while scattering from wave functions with a larger out-of-plane orbital component is suppressed (enhanced). Applying this to the ideal $j_{\text{eff}} = \frac{3}{2}$ wave functions, which can be expressed as $|\frac{3}{2}, \pm\frac{3}{2}\rangle = (\mp|d_{yz}, \pm\sigma\rangle + i|d_{xz}, \pm\sigma\rangle)/\sqrt{2}$ and $|\frac{3}{2}, \pm\frac{1}{2}\rangle = (\mp|d_{yz}, \mp\sigma\rangle + i|d_{xz}, \mp\sigma\rangle + 2|d_{xy}, \pm\sigma\rangle)/\sqrt{6}$, we expect grazing incidence to result in a preferential enhancement of excitations associated with the $j_z = \pm\frac{1}{2}$ states.

As illustrated in Fig. 3(a), the orbital excitations of Ba_2IrO_4 in grazing incidence are markedly different from those of Sr_2IrO_4 measured in the same geometry, but bear a striking

resemblance to those of Sr_2IrO_4 measured in normal incidence [see Fig. 2(b) in Ref. [31]]. The grazing incidence data in Fig. 3(a) imply that the $j_z = \pm\frac{1}{2}$ levels form the lower-energy $j_{\text{eff}} = \frac{3}{2}$ states in Ba_2IrO_4, but the higher-energy states in Sr_2IrO_4. This energy level scheme is illustrated in Fig. 3(b). Note that this scheme implies that the sign of the effective noncubic crystal field splitting (Δ_{CEF}) must be opposite in Ba_2IrO_4 and Sr_2IrO_4, despite the fact that both materials display a similar elongation of IrO_6 octahedra. Since this octahedral distortion is expected to generate a positive tetragonal crystal field splitting in both systems, the apparent reversal of $j_{\text{eff}} = \frac{3}{2}$ levels demonstrates that longer-range crystal field effects must play a significant role in these materials as pointed out in Ref. [19]. This reversal of energy levels is consistent with recent x-ray absorption measurements on Ba_2IrO_4 [32] and Sr_2IrO_4 [33].

A comparison of excitation spectra for Ba_2IrO_4 (glancing geometry) and Sr_2IrO_4 (normal geometry, as in Ref. [31]) also reveals a clear suppression of the spin-orbit exciton energy scale. The sharp exciton feature at $\mathbf{Q} = (\pi/2, \pi/2)$ shifts from ∼470 meV in Sr_2IrO_4 to ∼350 meV in Ba_2IrO_4. This trend is opposite to predictions from quantum chemistry calculations [17], and approximately four times larger than predicted by theory. This peak shift seems to be due to the larger bandwidth of the spin-orbit exciton in Ba_2IrO_4, as the zone center energy of ∼600 meV is similar to that in Sr_2IrO_4 [see Fig. 3(d)]. We note that the observed bandwidth of ∼250 meV in Ba_2IrO_4 is almost a factor of two larger than that of Sr_2IrO_4. However, the apparent larger bandwidth could be due to the presence of two spin-orbit exciton modes and a further investigation of the incident angle dependence is necessary to disentangle these two modes, as was done for Sr_2IrO_4 [31].

The strain dependence of the spin-orbit exciton mode [Figs. 2(c) and 2(d)] suggests that epitaxial strain can also be used to tune the orbital properties of Ba_2IrO_4. As the compressive strain increases, we expect the c/a ratio to grow larger and the elongation of the IrO_6 octahedra to become more pronounced. This octahedral distortion should make the noncubic crystal field splitting Δ_{CEF} larger in Ba_2IrO_4 [see Fig. 3(b)]. In principle, this suggests that it should be possible to tune Ba_2IrO_4 (or Sr_2IrO_4) to the $\Delta_{\text{CEF}} = 0$ limit where the magnetic anisotropy vanishes, by applying an appropriate epitaxial strain. In the case of Ba_2IrO_4 the required strain should be tensile (to decrease Δ_{CEF}), while for Sr_2IrO_4 it should be compressive (to increase Δ_{CEF}). This conclusion is supported by recent local density approximation plus dynamical mean-field theory (LDA+DMFT) calculations on Sr_2IrO_4 [34], which predict that a compressive strain of ∼1% would be required to tune the local structure to the $\Delta_{\text{CEF}} = 0$ point. It is interesting to note that the $\Delta_{\text{CEF}} = 0$ limit in Ba_2IrO_4 and Sr_2IrO_4, which restores full rotational symmetry, does not correspond to perfectly undistorted IrO_6 octahedra, but rather to the point where short-range and long-range crystal field effects cancel out.

V. SUMMARY AND CONCLUSIONS

In summary, our RIXS studies of ultrathin epitaxial films of Ba_2IrO_4 reveal that the bandwidths of the low-energy magnetic and spin-orbit excitations in this material are significantly larger than those found in Sr_2IrO_4. This observation can be understood from the increased hopping due to the 180° Ir-O-Ir bond in Ba_2IrO_4, which suggests that itinerancy may be important for understanding the electronic structure of Ba_2IrO_4. The results of this study demonstrate that hard x-ray RIXS can provide a detailed probe of spin and orbital excitations in ultrathin film samples. This technique offers unique opportunities for the study of samples which are difficult, or impossible, to synthesize in bulk single crystal form, allowing novel materials to be investigated under a variety of highly tunable strain conditions (tensile or compressive, uniform or anisotropic). In closing, we note that the relatively high inelastic count rates in this study (∼5 counts/s) resulted in very reasonable measurement times (∼1–2 minutes per point for the data in Figs. 2 and 3). This suggests that measurements on monolayer and bilayer thin films are entirely feasible even with hard x rays, opening up exciting possibilities for the study of multilayers, buried interfaces, and complex heterostructures.

ACKNOWLEDGMENTS

We thank J. van den Brink for invaluable discussions. Work at the University of Toronto was supported by the Natural Sciences and Engineering Research Council (NSERC) of Canada, the Banting Postdoctoral Fellowship program, and the Canada Research Chairs program. Work at Cornell University was supported by the Air Force Office of Scientific Research (Grant No. FA9550-21-1-0168), and the National Science Foundation (No. DMR-2104427). M.U. acknowledges the support by the JSPS Postdoctoral Fellowships for Research Abroad. Use of the Advanced Photon Source at Argonne National Laboratory is supported by the U.S. Department of Energy, Office of Science, Office of Basic Energy Sciences, under Contract No. DE-AC02-06CH11357.

[1] B. J. Kim, H. Jin, S. J. Moon, J.-Y. Kim, B.-G. Park, C. S. Leem, J. Yu, T. W. Noh, C. Kim, S.-J. Oh *et al.*, Phys. Rev. Lett. **101**, 076402 (2008).

[2] B. J. Kim, H. Ohsumi, T. Komesu, S. Sakai, T. Morita, H. Takagi, and T. Arima, Science **323**, 1329 (2009).

[3] G. Jackeli and G. Khaliullin, Phys. Rev. Lett. **102**, 017205 (2009).

[4] G. Cao and P. Schlottmann, Rep. Prog. Phys. **81**, 042502 (2018).

[5] J. Bertinshaw, Y. Kim, G. Khaliullin, and B. Kim, Annu. Rev. Condens. Matter Phys. **10**, 315 (2019).

[6] F. Wang and T. Senthil, Phys. Rev. Lett. **106**, 136402 (2011).

[7] H. Watanabe, T. Shirakawa, and S. Yunoki, Phys. Rev. Lett. **110**, 027002 (2013).

[8] J. Kim, D. Casa, M. H. Upton, T. Gog, Y.-J. Kim, J. F. Mitchell, M. van Veenendaal, M. Daghofer, J. van den Brink, G. Khaliullin *et al.*, Phys. Rev. Lett. **108**, 177003 (2012).
[9] Y. Yang, W.-S. Wang, J.-G. Liu, H. Chen, J.-H. Dai, and Q.-H. Wang, Phys. Rev. B **89**, 094518 (2014).
[10] H. Okabe, M. Isobe, E. Takayama-Muromachi, A. Koda, S. Takeshita, M. Hiraishi, M. Miyazaki, R. Kadono, Y. Miyake, and J. Akimitsu, Phys. Rev. B **83**, 155118 (2011).
[11] S. Boseggia, R. Springell, H. C. Walker, H. M. Rønnow, C. Rüegg, H. Okabe, M. Isobe, R. S. Perry, S. P. Collins, and D. F. McMorrow, Phys. Rev. Lett. **110**, 117207 (2013).
[12] S. Moser, L. Moreschini, A. Ebrahimi, B. D. Piazza, M. Isobe, H. Okabe, J. Akimitsu, V. V. Mazurenko, K. S. Kim, A. Bostwick *et al.*, New J. Phys. **16**, 013008 (2014).
[13] M. Moretti Sala, M. Rossi, A. Al-Zein, S. Boseggia, E. C. Hunter, R. S. Perry, D. Prabhakaran, A. T. Boothroyd, N. B. Brookes, D. F. McMorrow *et al.*, Phys. Rev. B **90**, 085126 (2014).
[14] M. Uchida, Y. F. Nie, P. D. C. King, C. H. Kim, C. J. Fennie, D. G. Schlom, and K. M. Shen, Phys. Rev. B **90**, 075142 (2014).
[15] I. V. Solovyev, V. V. Mazurenko, and A. A. Katanin, Phys. Rev. B **92**, 235109 (2015).
[16] K. Rościszewski and A. M. Oleś, Phys. Rev. B **93**, 085106 (2016).
[17] V. M. Katukuri, H. Stoll, J. van den Brink, and L. Hozoi, Phys. Rev. B **85**, 220402(R) (2012).
[18] S. Tsuda, H. Okabe, M. Isobe, and S. Uji, J. Phys. Soc. Jpn. **85**, 023703 (2016).
[19] N. A. Bogdanov, V. M. Katukuri, J. Romhanyi, V. Yushankhai, V. Kataev, B. Büchner, J. van den Brink, and L. Hozoi, Nat. Commun. **6**, 7306 (2015).
[20] V. M. Katukuri, V. Yushankhai, L. Siurakshina, J. van den Brink, L. Hozoi, and I. Rousochatzakis, Phys. Rev. X **4**, 021051 (2014).
[21] Y. S. Hou, H. J. Xiang, and X. G. Gong, New J. Phys. **18**, 043007 (2016).
[22] J. Nichols, O. B. Korneta, J. Terzic, G. Cao, J. W. Brill, and S. S. A. Seo, Appl. Phys. Lett. **104**, 121913 (2014).
[23] Y.-Q. Zhao, H. Zhang, X.-B. Cai, W. Guo, D.-X. Ji, T.-T. Zhang, Z.-B. Gu, J. Zhou, Y. Zhu, and Y.-F. Nie, Chin. Phys. B **30**, 087401 (2021).
[24] L. Braicovich, L. J. P. Ament, V. Bisogni, F. Forte, C. Aruta, G. Balestrino, N. B. Brookes, G. M. De Luca, P. G. Medaglia, F. Miletto Granozio, M. Radovic, M. Salluzzo, J. van den Brink, and G. Ghiringhelli, Phys. Rev. Lett. **102**, 167401 (2009).
[25] J. Schlappa, K. Wohlfeld, K. Zhou, M. Mourigal, M. Haverkort, V. Strocov, L. Hozoi, C. Monney, S. Nishimoto, S. Singh *et al.*, Nature (London) **485**, 82 (2012).
[26] G. Cao, J. Bolivar, S. McCall, J. E. Crow, and R. P. Guertin, Phys. Rev. B **57**, R11039 (1998).
[27] See Supplemental Material at http://link.aps.org/supplemental/10.1103/PhysRevB.107.054423 for a detailed discussion of the magnetic structure of the thin film samples.
[28] A. Lupascu, J. P. Clancy, H. Gretarsson, Z. Nie, J. Nichols, J. Terzic, G. Cao, S. S. A. Seo, Z. Islam, M. H. Upton *et al.*, Phys. Rev. Lett. **112**, 147201 (2014)
[29] R. Coldea, S. M. Hayden, G. Aeppli, T. G. Perring, C. D. Frost, T. E. Mason, S.-W. Cheong, and Z. Fisk, Phys. Rev. Lett. **86**, 5377 (2001).
[30] A. Seo, P. P. Stavropoulos, H.-H. Kim, K. Fürsich, M. Souri, J. G. Connell, H. Gretarsson, M. Minola, H. Y. Kee, and B. Keimer, Phys. Rev. B **100**, 165106 (2019).
[31] J. Kim, M. Daghofer, A. H. Said, T. Gog, J. van den Brink, G. Khaliullin, and B. J. Kim, Nat. Commun. **5**, 4453 (2014).
[32] M. Moretti Sala, M. Rossi, S. Boseggia, J. Akimitsu, N. B. Brookes, M. Isobe, M. Minola, H. Okabe, H. M. Rønnow, L. Simonelli, D. F. McMorrow, and G. Monaco, Phys. Rev. B **89**, 121101(R) (2014).
[33] D. Haskel, G. Fabbris, M. Zhernenkov, P. P. Kong, C. Q. Jin, G. Cao, and M. van Veenendaal, Phys. Rev. Lett. **109**, 027204 (2012).
[34] H. Zhang, K. Haule, and D. Vanderbilt, Phys. Rev. Lett. **111**, 246402 (2013).